Fabrication of fibers with high rare-earth concentrations for Faraday isolator applications

John Ballato and Elias Snitzer

The Faraday effect provides a mechanism for achieving unidirectional light propagation in optical isolators; however, miniaturization requires large Verdet constants. High rare-earth content glasses produce suitably large Verdet values, but intrinsic fabrication problems remain. The novel powder-in-tube method, or a single-draw rod-in-tube method, obviates these difficulties. The powder-in-tube method was used to make silica-clad optical fibers with a high terbium oxide content aluminosilicate core. Core diameters of 2.4 μm were achieved in 125-μm-diameter fibers, with a numerical aperture of 0.35 and a Verdet constant of -20.0 rad/(T m) at 1.06 μm. This value is greater than 50% for crystals found in current isolator systems. This development could lead to all-fiber isolators of dramatically lower cost and ease of fabrication compared with their crystalline competitors.

1. Introduction

Modern photonic devices for optical computing, telecommunications, etc., require classes of elements that exhibit nonreciprocal behavior. One such class is based on the Faraday effect,[1] in which the rotation of plane-polarized light is dependent on only the applied magnetic field and is not dependent on the direction of light propagation. This provides unidirectional propagation of light in an optical fiber. In this paper we briefly describe this effect to illustrate the factors that influence the Verdet constant,[2] characterizing the magnitude of the effect, and our choice of the high rare-earth content glass composition for its attainment. This is followed by a short discussion of a novel method of fabricating optical fibers with these constituents and the experimental realization of fibers with large Verdet constants.

2. Faraday Effect

The Faraday effect in glass is a well-understood phenomenon and has been intensively studied and documented.[3–10] It is present in all materials and is closely related to the magnetic behavior of the component ions. The rotation varies with temperature in paramagnetic and ferromagnetic materials, but is temperature independent in diamagnetic materials. Its magnitude also tends to decrease with increasing wavelength. The Faraday effect is a magnetic-field-induced circular birefringence, providing a means of controlling the polarization state of light. The effect is distinct from intrinsic circular birefringence (optical chiralty or activity) in that its rotation direction depends on only the direction of the magnetic field along the path of light propagation and not on the direction of light propagation. The optical rotation arises from the inequality of the refractive indices for right- and left-circularly polarized light; these, in turn, stem from the ground- and excited-state splitting in the medium when an external magnetic field is applied.

At a more fundamental level, Faraday rotation can be implicitly inferred from the time-reversal asymmetry of Maxwell's equations. These are

$$\nabla \times \mathbf{E} = -\frac{\partial \mathbf{B}}{\partial t},$$

$$\nabla \times \mathbf{H} = \frac{\partial \mathbf{D}}{\partial t} + \mathbf{J},$$

$$\nabla \cdot \mathbf{D} = \rho,$$

$$\nabla \cdot \mathbf{B} = 0.$$

When (t) is replaced with $(-t)$ for $\mathbf{E}$ and $\mathbf{D}$, this is equivalent to replacing x, y, and z by $(-x)$, $(-y)$, and $(-z)$, respectively [similarly, $\mathbf{r}$ by $(-\mathbf{r})$]. The physical

The authors are with the Fiber Optic Materials Research Program, Rutgers, The State University of New Jersey, Piscataway, New Jersey 08855-0909.

Received 21 November 1994; revised manuscript received 31 March 1995.

0003-6935/95/306848-07$06.00/0.

implication is that time reversal causes a similar reversal in the directions of **E** and **D** (i.e., they retrace their values in amplitude and polarization). However, for the magnetic field to be retraced, the orientation of **B** must be reversed. Therefore in Faraday isolator systems in which **B** is not replaced by $(-\mathbf{B})$, we achieve the unique behavior that separates the Faraday effect from the natural optical rotation found in chiral crystals and other enantiomorphous materials. The existence of Faraday rotation in all materials stems directly from this proof (i.e., light's electromagnetic interaction with any media is determined by Maxwell's equations coupled with the proper material constitutive equations).

The rotation in the plane of polarization, Θ, may be represented as

$$\Theta = V \int \mathbf{B} \cdot \mathrm{d}l,$$

where V is defined by this equation as a material parameter known as the Verdet constant, **B** is the applied axial magnetic flux density,[11] and $\mathrm{d}l$ is the differential length along the propagation path exposed to the magnetic field.

The Faraday effect per unit length can be alternatively defined as

$$\Theta = \frac{\omega}{2c}(n_- - n_+),$$

where n_- and n_+ are the refractive indices for left- and right-circularly polarized light of angular frequency ω. The expressions for n_- and n_+ can be obtained from Maxwell's equations, combined with the constitutive equations for conductivity and dielectric constant. From this it follows[11] that

$$V = \frac{Ne^3}{2nm^2}\frac{1}{c\epsilon_0}\frac{\omega^2}{(\omega^2 - \omega_0{}^2)^2}$$

for a material of electronic resonant frequency ω_0 and nominal refractive index n, with N charge carriers per unit volume of charge e and mass m, operating at a wavelength $\lambda = (2\pi c/\omega)$ (the case for an undamped harmonic oscillator that gives rise to a resonant denominator). Depending on the magnetic nature of the isolator material, simplifications to the above equation may be made. These simplifications are addressed below for two broad classes of optical materials.

Faraday rotation has a number of significant practical applications. It lends itself to the construction of optical switches, modulators, circulators, field sensors, and optical isolators. The optical isolator greatly benefits from high Verdet constant materials. Isolators are analogous to electronic diodes, permitting light propagation in one direction only. In these devices, the incident-plane polarized light is passed through a Faraday rotating material in a magnetic field so as to produce a 45° rotation of the polarization plane. It is then transmitted through a polarization analyzer oriented at 45° with respect to the first polarizer. A schematic of this configuration is depicted in Fig. 1. Backreflected light traversing in the opposite direction experiences an added 45° rotation, leading to a polarization in the direction blocked by the first polarizer. This is important in sensitive laser systems in which backreflected radiation is detrimental to the laser source, as well as in fiber laser schemes in which reflected pulses experience gain with each amplifier pass causing ghosted signals. There are several factors that affect the extent of attenuation. Among the most important are inhomogeneities in the magnetic field, in the refractive index, and in the magnetic ion distribution. To achieve specified rotations with a minimum of material and with magnetic fields as low as possible, the Verdet constant should be as large as possible.

The classical Verdet relation for diamagnetic materials was derived by Becquerel.[12] It showed the rotation to be linearly dependent on the optical dispersion. The form often given, in cgs units normalized to the magnetic intensity **H**, rather than the preferable definition[11] in terms of the flux density given above, is

$$V = \frac{e\lambda}{2mc^2}\frac{\mathrm{d}n}{\mathrm{d}\lambda},$$

where e and m are the charge and the mass, respectively, of the electron, c is the speed of light, and $\mathrm{d}n/\mathrm{d}\lambda$ is the refractive-index dispersion with wavelength. This equation holds closely for most diamagnetic materials. A factor γ called the magneto-optic anomaly, is often used as a multiplier to account for the nature of the chemical bond in these diamagnetic materials. The anomaly factor ranges from roughly $1/4$ for highly covalent bonds (e.g., diamond) to approximately unity for ionic bonding (e.g., ZnS).

In dealing with paramagnetic materials or materials with both diamagnetic and paramagnetic species (as is the case with rare-earth aluminosilicate glasses), other terms must be included to account for the magnetic susceptibilities of the paramagnetic ions. In those materials, the Verdet constant is propor-

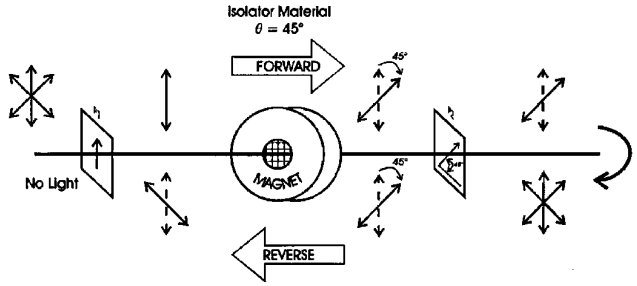

Fig. 1. Schematic of a bulk Faraday rotation isolator configuration with electromagnetic polarization states.

tional to[13,14]

$$\nu^2\left[\sum_i \frac{A_i}{(\omega_i^2 - \omega^2)^2} + \sum_i \sum_j \frac{B_{ij}}{(\omega_i^2 - \omega^2)(\omega_j^2 - \omega^2)}\right] = \nu^2(D + P),$$

where ν is the frequency of the light, D is the diamagnetic component that can be simply calculated from the Becquerel equation, and P is the paramagnetic component that can be calculated from quantum-mechanical considerations of the ground- and excited-state splitting.[6]

3. Rare-Earth Glasses

Suitably large Verdet constants are possible in diamagnetic glasses (e.g., As_2S_3); however, paramagnetic glasses that contain certain rare-earth ions in high concentrations are preferred because of the glasses' greater durability and lower absorption in the spectral regions of interest. In these rare-earth-doped glasses, the rotation involves the $4f$–$5d$ virtual electronic electric-dipole transition, which is a function of atomic number. At high concentrations, the Verdet constant is approximately linear with concentration. High rare-earth content glasses should, therefore, yield large magneto-optic rotations. However, the concentration of paramagnetic ions that can be added to a glass is limited by its glass-forming properties. Advantages of doped aluminosilicate glasses include their high solubilities for rare-earth species, their compatibility with pure silica claddings, and their capacity for splicing into existing fiber networks.

Most glasses that contain trivalent rare-earth ions, although transparent in some regions, typically have numerous absorption lines extending from the near infrared to the near ultraviolet. In contrast to this, Ce^{3+}, Gd^{3+}, Yb^{3+}, and Tb^{3+} are transparent in the visible and near infrared. The energy-level diagrams for Tb^{3+} as well as for Ce^{3+}, Gd^{3+}, and Yb^{3+} are depicted in Fig. 2. The Tb^{3+} ion is transparent from the green down to 1.6 μm and has the largest Faraday rotation per ion.[6] It is for these reasons that terbium aluminosilicates are indicated as materials of special importance.

4. Powder-in-Tube Method

Traditional preform fabrication techniques (e.g., modified chemical vapor deposition) limit rare-earth concentrations to approximately 15 wt% because of the resultant thermal expansion mismatch from the necessary addition of aluminum to promote solubility and dispersion of the rare-earth species. Fibers with high rare-earth content cores have also been made by the selective volatization method.[15] Fabrication of high rare-earth content glasses typically uses a batching technique.[16] This calls for the weighing and mixing of component powders that ultimately are melted in a crucible. This melt then is poured into a rod-shaped mold. After cooling to an amorphous solid, the rod subsequently is inserted in a tube and drawn into a fiber. Great care is required for reduc-

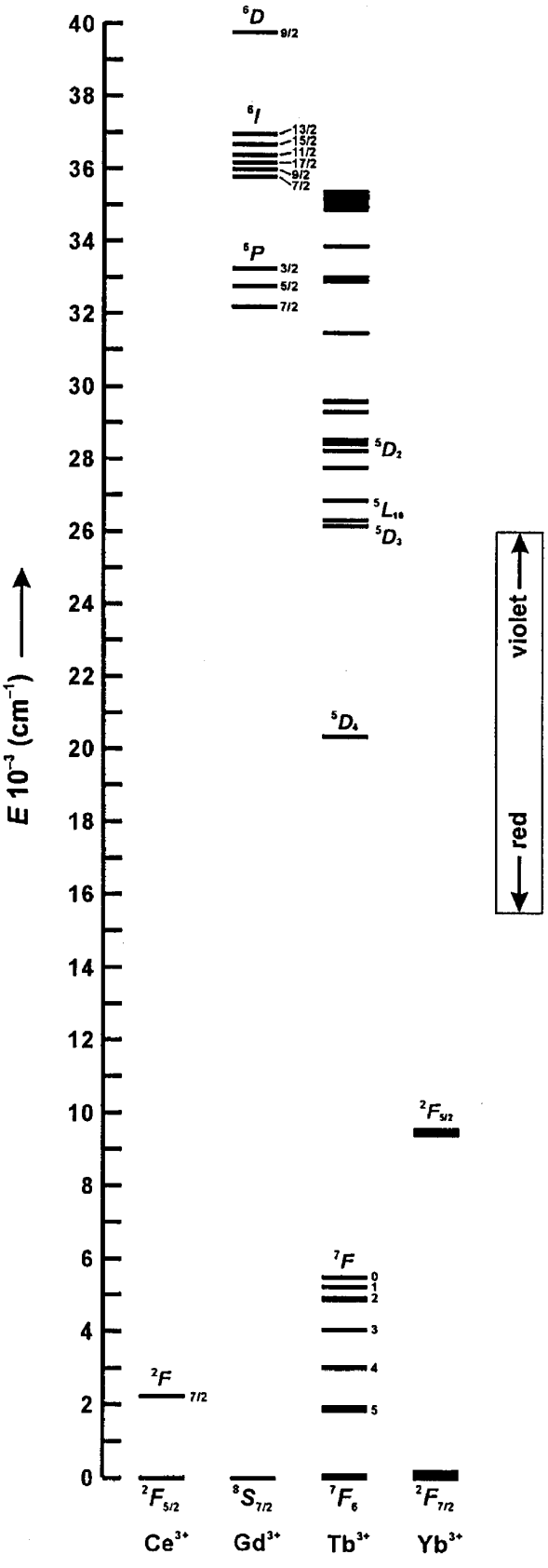

Fig. 2. Electronic energy-level diagram for Ce^{3+}, Gd^{3+}, Tb^{3+}, and Yb^{3+}. Note transparency in the visible region.

ing crucible contamination for low-loss optical fiber systems. An alternative approach is the powder-in-tube method outlined below.

To overcome the crucible contamination problems associated with core-glass fabrication before fiber drawing, it was considered that melting the powder composition in a silica capillary tube during the draw process could circumvent this problem. This technique has been termed the powder-in-tube process. The powder-in-tube process calls for chemical reduction of the rare-earth powder to the trivalent state and intimate mixing of the powders to enhance the melt characteristics. The formulation is similar to that of the batch process, but the composition is then inserted into the hollow core of a silica capillary tube. Certain applications necessitate specific core–clad diameter ratios. This requirement may be accommodated in several ways. One may resleeve the powder-filled capillary into a second glass tube or cane; this still requires but a single draw. When large clad-to-core ratios are desired, one may alternatively start with a small capillary inside a large one. A schematic representation of the latter arrangement is shown in Fig. 3. On drawing this powder-filled capillary into an optical fiber, the high rare-earth content center melts to a fluent liquid that then solidifies to a glassy core when the fiber cools. The capillary actually acts as a silica crucible for melting, but ultimately draws into the fiber cladding as the fabrication progresses. Because the capillary is pure silica and the core glass is an aluminosilicate, the diffusion of silica between the core and the clad is not viewed as a contamination detrimental to the optical properties of the fiber. If the diffusion were excessive it would lower the numerical aperture and the Verdet constant. Although some diffusion does occur, we did not think it was a troublesome amount.

5. Experimental Results

The fabrication of optical fibers that contained a high rare-earth concentration required several stages. As mentioned, the trivalent rare-earth ions have the largest paramagnetic Faraday rotation.[17] One of the highest rotation per ion is realized in Tb^{3+}, and it is transparent over wide sections of the visible and near-infrared regions. For this reason Tb_2O_3 was chosen as the rare-earth oxide powder component to be investigated. Commercially available is the higher oxide Tb_4O_7; this is presumably $Tb_2O_3 \cdot 2TbO_2$, with an unacceptable mixed valency of Tb^{3+} and Tb^{4+} ions. The literature shows[18] that Tb_4O_7 will reduce to Tb_2O_3 at approximately 800 °C in a nitrogen or hydrogen atmosphere. Samples were reduced in a carbon crucible at 800 °C for 5 h under an ultrahigh-purity nitrogen atmosphere. Powder x-ray diffraction analysis of this sample showed excellent correlation with the existing diffraction pattern for pure Tb_2O_3.

Fibers that contained 54 wt.% Tb_2O_3, 27 wt.% SiO_2, 18 wt.% Al_2O_3, and 1 wt.% Sb_2O_3 (as a fining agent) were successfully produced by the powder-in-tube procedure. A complete fusion between the silica cane and capillary was observed in a test section of 250 m of fiber. This optical assessment agreed well with electron microscopy results, which indicated core–clad fusion without interfacial crystallization. A major concern was that unfined bubbles would be found in the core. These could lead to voids in the drawn fiber. This concern did not turn out to be a problem, as no scattering centers could be visually observed. The test section contained a continuous high rare-earth concentration core, which had cooled from a melt at the preform neckdown region.

The numerical aperture, which is a measure of the angle for light acceptance and emission in and out of the fiber core, was determined for the powder-in-tube sample to be 0.35. From the definition of the numerical aperture, the core glass refractive index was 1.50 (at 632.8 nm). An index of 1.62 was determined by ellipsometry on a bulk sample. These index differences are attributed to diffusion of silica between the core and the cladding.

We observed optical waveguide modal patterns on viewing sample fiber lengths under a light microscope in transmission. The low-order modes (TE_{02}, TM_{02}, or HE_{22}) were clear and easily distinguishable in the red end of the visible spectrum, from which we conclude that there was only limited scattering of the propagation modes. Aluminum in the core composition lowers the melt viscosity, thereby producing an increased constituent diffusion and a radial refractive-index grading (Figs. 4 and 5). The existence of a graded index across the fiber diameter causes a lower

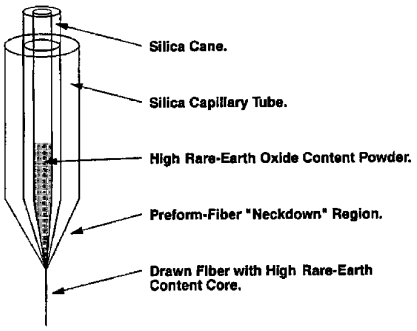

Fig. 3. Schematic of powder-in-tube method for the fabrication of high rare-earth content optical fibers.

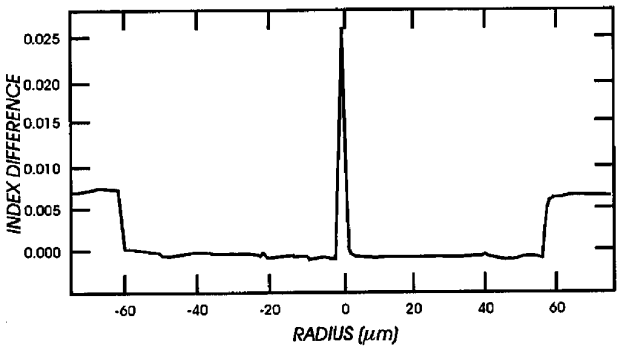

Fig. 4. Refractive-index profile of powder-in-tube fiber (125-μm diameter).

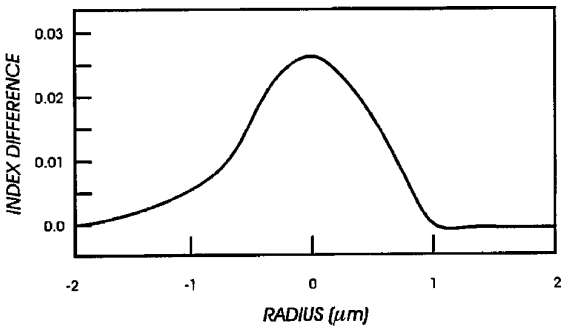

Fig. 5. Refractive-index profile of powder-in-tube fiber core region. Note distribution indicative of diffusional processes (profile asymmetry from instrumental optical aberrations).

effective numerical aperture and larger modal pattern diameters. From the fact that the modal patterns were easily viewed and resolved, we conclude that the core glass had homogeneously mixed and fined as it progressed from the powder stage, through the melt, to the glassy core. Poorly mixed glass would produce scattering among all the propagation modes, and simple mode patterns would not be observed. The powder-to-glass transition is shown in Fig. 6.

Optical absorption measurements were attempted on a several-meters length of fiber. Spectral losses were too high over this length, whereas shorter fiber lengths were not long enough to yield accurate loss results. Fiber samples of 10 cm were viewed, as mentioned above, under a transmission light microscope, and waveguide modal patterns, consistent with a symmetric-step geometry,[19] were easily viewed. The existence of high loss is attributed to the purity of the starting powders and not to axially irregular core–clad interdiffusion. Powders utilized for both bulk preparation and fiber fabrication were of 99% purity. Bulk samples 3 mm thick exhibited a broad absorption centered at approximately 1 μm; this is attributed primarily to Fe^{2+} and, secondarily, to Cu^{2+} [30 parts in 10^6 (ppm) in Tb_4O_7]. Problems concerning excessive loss over long fiber lengths are not considered severe, as the large Verdet constants for the terbium aluminosilicate treated here set the usable isolator length at roughly double (or approximately 20 cm) that of the crystalline alternative.

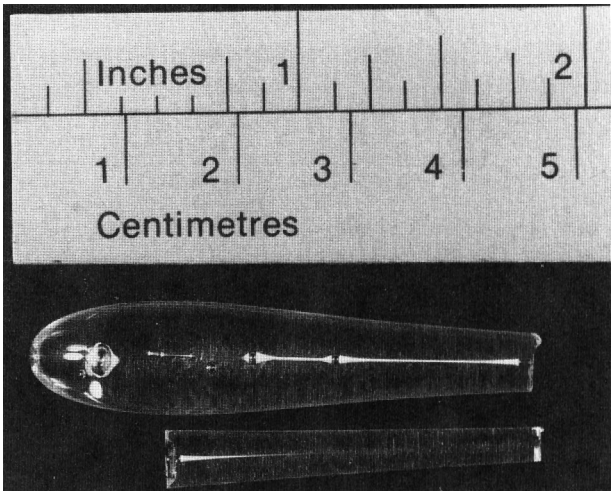

Fig. 6. Optical micrograph of powder-to-glass transition in powder-in-tube core region.

Differential thermal analysis (DTA) of the bulk sample indicated a refractory glass with a melting point of approximately 1340 °C. This is important because the powder-in-tube method requires that the core glass melt at a temperature lower than that at which the clad glass softens, and this indeed was the case. The thermal expansion coefficient of the terbium aluminosilicate core glass measured by thermomechanical analysis (TMA) was found to be approximately 4.4×10^{-6}/K over the range of 45 to 600 °C. Table 1 summarizes the physical properties of the glass composition treated in this paper.

A commercial vendor, Isowave Inc.,[20] performed Verdet constant measurements on a bulk terbium aluminosilicate glass sample. Their experimentally determined room-temperature Verdet constant was found to be $V = -20.0$ rad/(T m) at 1.06 μm. This is more than one half of the Verdet constant of commercially available crystals used in optical isolators. Figure 7 graphs the traditional variation in Verdet constant with wavelength for the terbium aluminosilicate and a commercial rare-earth garnet crystal [terbium gallium garnet (TGG)] used in isolator applications. Table 2 lists the Verdet values for these two materials as a function of wavelength. Using the classical approximation[10,21] for the wavelength dependence of V,

$$V = \frac{A}{\lambda^2 - {\lambda_0}^2},$$

we find from a least-squares fit ($r^2 = 0.994$) to the data of Fig. 7 that $A \approx -19.7 \times 10^6$ [(nm)^2 × rad/(T m)]and $\lambda_0 \approx 385$ nm. This represents a departure from the published values for the Tb^{3+} ion of 250 nm[21] and 215 nm.[10] Berger *et al.*[10] indicate that λ_0 does not necessarily represent only one transition responsible for Faraday rotation, but is a weighted average

Table 1. Physical Properties of Terbium Aluminosilicate Glass

Composition	
Tb_2O_3	54 wt.%
SiO_2	27 wt.%
Al_2O_3	18 wt.%
Sb_2O_3	1 wt.%
Glass transition temperature	880 °C
Crystallization temperature	1090 °C
Melting temperature	1340 °C
Coefficient of thermal expansion	4.4×10^{-6}/K
Density	3.3×10^3 kg/m^3
Bulk refractive index at 632.8 nm	1.62
Verdet constant at 1.06 μm	−20.0 rad/(T m)[a]
Fiber numerical aperture	0.35

[a]In cgs emu, the Verdet constant at 1.06 μm = −0.069 min/(Oe cm). The cgs (emu) to mks conversion is V[rad/(T m)] = (25/27)π × 100 V[min/(Oe cm)].

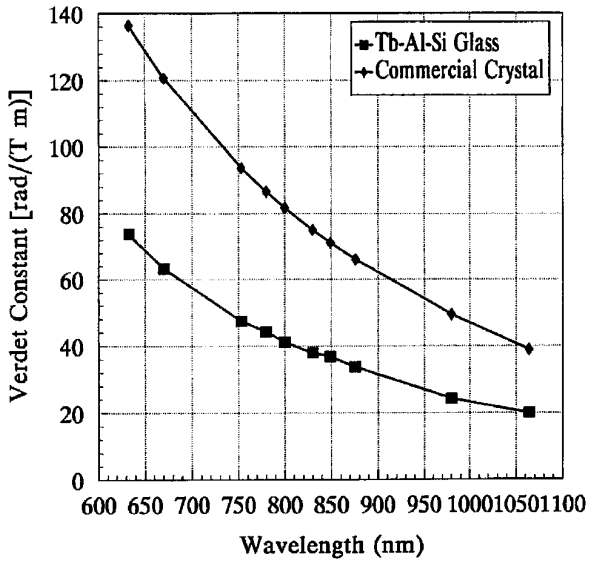

Fig. 7. Verdet constant [rad/(T m)] versus wavelength (nanometers) for a bulk terbium aluminosilicate sample and a commercially available TGG isolator crystal.

of the real transition wavelengths. The averaging reflects the relative transition strengths and deviations from the observation frequency. The effective transition wavelength, λ_0, is exact only when there is but one transition. The variation in λ_0 values arises from the differing terbium concentrations and the glass hosts. The A parameter above is not simply a formula constant, but rather is a function of temperature, *concentration,* and effective dipole matrix elements. The previously published values for A correspond to Tb^{3+} concentrations of 3.8×10^{21} ions/cm^3 and 5.4×10^{21} ions/cm^3, which are, respectively,

Table 2. Verdet Constant versus Wavelength for Terbium Aluminosilicate Glass and Commercial TGG Isolator Crystal

Wavelength (nm)	Verdet Constant[a] for Terbium Aluminosilicate [rad/(T m)]	Verdet Constant for TGG Crystal [rad/(T m)]	Ratio of Glass/Crystal Verdet Constants
633	−73.723	−136.306	0.541
670	−63.191	−120.686	0.524
753	−47.393	−93.634	0.506
780	−44.234	−86.566	0.511
800	−41.074	−81.737	0.502
830	−37.915	−75.076	0.505
849	−36.861	−71.178	0.518
876	−33.702	−66.030	0.510
980	−24.223	−49.450	0.490
1064	−20.010	−38.891	0.515

[a]Negative values for the Verdet constants correspond to a paramagnetic-ion-dominated rotation. Diamagnetic ions result in positive rotations. The sense of the rotation is determined by the change in polarization direction with respect to the direction of current producing the magnetic field. Positive Verdet values mean that the change in the plane of polarization is in the same sense as the electric current producing the B field. Negative values imply an opposite correlation.

57%[21] and 82%[10] of the 6.6×10^{21} ions/cm^3 used in this study.

Further comparison[22] of the terbium aluminosilicate treated here with other Faraday rotator materials may be made from the seminal paper of Weber.[5] Table B of Ref. 5 contrasts the Verdet constants of various glasses and crystals at 1.06 μm. The −20.0 rad/(T m) Verdet constant of the 54 wt.% terbium aluminosilicate glass is comparable with the −20.6 rad/(T m) value for a terbium borosilicate glass. The aluminosilicate composition then ranks fourth on Weber's list in terms of amorphous rotator materials and first in terms of aluminosilicates or non-boron-containing silicate glasses.

6. Conclusion

For nonreciprocal applications, e.g., Faraday isolators, terbium aluminosilicate glasses are strongly indicated as future material systems of choice. Currently, terbium glasses are used in Faraday isolators at the Lawrence Livermore Laboratory's large neodymium oscillator–amplifier laser. The novel fabrication technique called the powder-in-tube method was successfully applied to the production of silica-clad fibers containing more than 50 wt.% terbium oxide. These glasses exhibited Verdet constants of greater than 50% of that shown by the much more expensive commercially available crystalline alternative, which is also a miniature bulk configuration rather than a fiber form.

The powder-in-tube method is potentially applicable over a wide compositional range, including halides and chalcogenides, as the main requirement is that the core powder components melt to form glass before the clad glass softening at the preform-fiber neckdown region. Volatile constituents may, however, be a problem with halide glasses.

The powder-in-tube method also obviates a potential problem with traditional preform fabrication methods. The differential thermal expansion between silica cladding and doped-silica cores may lead to stress-induced mechanical failure during preform tube collapse. The powder form of the preform core allows a single draw directly to final fiber form with a small core diameter. The thermal expansion mismatch between core and cladding becomes less critical at small core sizes.

The powder-in-tube procedure can ultimately provide a method for fabricating high-purity, low-loss fibers and reduce contaminations consistently found with core glass fabrication in a crucible. The weak links in the process remain the components that comprise the powders. Impurities in the powders are manifested as impurities in the core glass, thereby increasing the optical loss. The possibility exists for ultrahigh-purity sol–gel powders to be used, making the powder-in-tube method extremely useful generally, but particularly so for the production of high rare-earth-content glasses.

This work would never have come to fruition without the assistance and valuable input from Todd Abel,

Paul Foy, Rajiv Datta, Jeff Bonja, Dave Machewirth, Jim Fajardo, and Matt Dejneka of the Fiber Optic Materials Research Program, members of the U.S. Army Research Laboratory, Fort Monmouth, N.J., as well as professors of Rutgers University's Department of Ceramics. We also recognize thoughtful and timely contributions from Norbert J. Kreidl. The authors thank the Fiber Optic Materials Research Program, Rutgers University, the Polaroid Corporation, Isowave Incorporated, and the New Jersey Commission on Science & Technology for their support.

References

1. M. Faraday, "On the magnetization of light, and the illumination of magnetic lines of force," Philos. Trans. R. Soc. London **1,** 104–123 (1846).
2. E. Verdet, "Recherches sur les propriétés optiques développées dans les corps transparents par l'action du magnétisme," Ann. Chim. Phys. **41,** 370–412 (1854).
3. J. E. Shelby and J. T. Kolhi, "Rare-earth aluminosilicate glasses," J. Am. Ceram. Soc. **73,** 39–42 (1990).
4. A. Makishima, M. Kobayashi, and T. Shimohira, "Formation of aluminosilicate glasses containing rare-earth oxides," J. Am. Ceram. Soc. **65,** C-210 (1982).
5. M. J. Weber, "Faraday rotator materials," Rep. M-103 (Lawrence Livermore National Laboratory, University of California, Livermore, Calif., 1982); M. J. Weber, "Faraday rotator materials for laser systems," in *Laser and Nonlinear Optical Materials,* L. G. DeShazer, ed., Proc. Soc. Photo-Opt. Instrum. Eng. **681,** 75–90 (1986); G. H. Dieke and H. M. Crosswhite, "The spectra of the doubly and triply ionized rare earths," Appl. Opt. **2,** 675–686 (1963).
6. N. F. Borelli, "Faraday rotation in glass," J. Chem. Phys. **41,** 3289–3293 (1964).
7. C. C. Robinson, "The Faraday rotation of diamagnetic glasses from 0.334 μm to 1.9 μm," Appl. Opt. **3,** 1163–1166 (1964).
8. M. Daybell, W. C. Overton, Jr., and H. L. Laquer, "The Faraday effect at low temperatures in terbium alumina silicate glasses," Appl. Phys. Lett. **11,** 79–81 (1967).
9. C. C. Robinson and R. E. Graf, "Faraday rotation in praseodymium, terbium, and dysprosium alumino silicate glasses," Appl. Opt. **3,** 1190–1191 (1964).
10. S. B. Berger, C. B. Rubinstein, C. R. Kurkjian, and A. W. Treptow, "Faraday rotation in rare-earth (III) phosphate glasses," Phys. Res. **133,** A723–A727 (1964).
11. A. Sommerfeld, *Optics,* Vol. IV of Lectures on Theoretical Physics Series (Academic, New York, 1964), p. 105.
12. H. Becquerel, "Ser une interprétation applicable au phénomène de Faraday et au phénomène de Zeeman," C. R. Acad. Sci. Ser. C **125,** 679–685 (1897).
13. J. H. Van Vleck, *The Theory of Electric and Magnetic Susceptibilities* (Oxford U. Press, New York, 1932), pp. 367–371; H. Cole, "Magneto-optic effects in glass. Part 1," J. Soc. Glass Technol. **34,** 220 (1950).
14. P. A. Schulz, "Wavelength-independent Faraday isolator," Appl. Opt. **28,** 4458–4464 (1989).
15. E. Snitzer and R. Tumminelli, "SiO_2-clad fibers with selectively volatized soft-glass cores," Opt. Lett. **14,** 757–759 (1989).
16. S. J. Collocott and K. N. R. Taylor, "Magneto-optical properties of erbium-doped soda glass," J. Phys. **11,** 2885–2893 (1978).
17. Y. R. Shen, "Faraday rotation of rare-earth ions. I. Theory," Phys. Rev. **133,** A511–A515 (1964).
18. M. W. Urban and B. C. Cornilsen, "Bonding anomalies in the rare earth sesquioxides," J. Phys. Chem. Solids **48,** 475–479 (1987).
19. E. Snitzer, "Cylindrical dielectric waveguide modes," J. Opt. Soc. Am. **5,** 491–498 (1961); E. Snitzer and H. Osterberg, "Observed dielectric waveguide modes in the visible spectrum," J. Opt. Soc. Am. **5,** 499–505 (1961).
20. Isowave Incorporated, 64 Harding Road, Dover, N.J. 07801.
21. G. T. Petrovskii, I. S. Edelman, T. V. Zarubina, A. V. Malakhovskii, V. N. Zabluda, and M. Yu. Ivanov, "Faraday effect and spectral properties of high-concentrated rare earth oxide glasses in visible and near UV region," J. Non-Cryst. Solids **130,** 35–40 (1991).
22. N. J. Kreidl, Santa Fe, N.M. 87501 (personal communication, 1994).